IEEE Access
Multidisciplinary | Rapid Review | Open Access Journal

Received 27 May 2024, accepted 19 June 2024, date of publication 27 June 2024, date of current version 8 July 2024.

Digital Object Identifier 10.1109/ACCESS.2024.3419810

RESEARCH ARTICLE

DFIG-Based WECS With Partial-Scale Converter: Efficiency, Cost, and Volume Comparison of SiC-Based and IGBT-Based Converter Solution

HUSSAIN A. HUSSAIN[1], (Member, IEEE), JELENA LONCARSKI[2], (Member, IEEE), LEPOSAVA B. RISTIC[3], (Member, IEEE), AND ALBERTO BELLINI[2], (Senior Member, IEEE)

[1]Department of Electrical Engineering, Kuwait University, Kuwait City 13060, Kuwait
[2]Department of Electrical, Electronic, and Information Engineering "Guglielmo Marconi," University of Bologna, 40136 Bologna, Italy
[3]School of Electrical Engineering, University of Belgrade, 11120 Belgrade, Serbia

Corresponding author: Hussain A. Hussain (h.hussain@ku.edu.kw)

ABSTRACT The green goals imposed by many countries and the increasing application of renewable energy systems are bringing power electronics to the center of attention. Of particular interest are the wide band-gap devices, as they offer important benefits when considering the efficiency increase and volume reduction. Consequently, they can be viably adopted in renewable energy sources. In this paper, a 2 MW Doubly Fed Induction Generator (DFIG) based Wind Energy Conversion System (WECS) with a bidirectional partial-scale frequency converter composed of two back-to-back converters is considered. The main contribution of the paper is a result of comprehensive comparisons conducted for the two systems: DFIG WECS based on a Si-IGBT converter and DFIG WECS based on a SiC-MOSFET converter in terms of efficiency, volume, and cost. The performed comparison is also a fair comparison, being the selected modules are of the same power ratings. In this way, the previously unspecified but valuable decision-making process regarding the selection of power electronic modules suitable for DFIGs is facilitated. The thermal analysis has been implemented in PLECS, together with the converter control. The realistic libraries obtained from the manufacturers have been included for different power modules. The findings highlight the advantages of employing the Silicon Carbide-based converter in terms of minimizing the size and cost of passive components. They also offer insights on what is needed in order to make the Silicon Carbide solution the absolute best candidate.

INDEX TERMS SiC devices, Si devices, wind energy converters, efficiency comparison, doubly-fed induction generator (DFIG), wind energy conversion system (WECS).

I. INTRODUCTION

The need for efficient and affordable renewable energy is driving the scientific community towards creating new technologies for producing electrical power. All renewable energy sources need to be stepped up consistently, especially wind energy, which has been increasing dramatically in recent years. In contemporary wind power applications, different combinations of machines and power converters have been used to fulfill the requirements for high reliability, grid integration stability, reactive power control, and extended lifetime of the installed equipment.

When it comes to modern wind energy conversion system (WECS) topologies, four main categories can be distinguished: fixed speed with a squirrel-cage induction generator and semi-variable speed with a wound rotor induction generator (Type 1 and 2), semi-variable speed with a partial power converter with doubly fed induction generator (DFIG) (Type 3), and full-variable speed with a full-scale power converter, usually with permanent magnet synchronous generator (PMSG) (Type 4) [1], [2], [3]. The common types for the new installations are Type 3 and 4 WECS. The main

The associate editor coordinating the review of this manuscript and approving it for publication was Yuh-Shyan Hwang.

difference between the two is that Type 4 WECS requires a full-scale converter, and the generator has only one set of three-phase windings connected to the grid, while DFIG WECS has two sets of windings: the main set of windings which is connected directly to the grid and where most power flows through, and the other set of windings connected to the grid through a power electronics converter with reduced power ratings. This is also the main benefit of such WECS, being the converter rating of approximately 25%-30% of the generator rating [4], making it, in this way, a cost-effective variable speed operation solution and independent active and reactive power control [5], [6]. On the other hand, the most important disadvantage of such a generator is the need for slip rings and brushes to provide power to the rotor circuit [7], even though the typical DFIG can generally fulfill all the posed requirements for WECS [8], [9], [10], [11]. Even though PMSG is heavier and larger than DFIG WECSs, the slip rings and gearbox can be eliminated by the use of the multi-pole structure of the generator [1]. These generators are known as direct-drive, and even though they have high energy yield, the cost is higher than in the other generator systems with gearbox, single or multi-stage [12]. On the other hand, a DFIG with a single-stage gearbox seems the most interesting choice in terms of energy yield divided by cost.

DFIG-based WECS feature power electronics converters with partial ratings, which can be seen as a benefit as it reduces the size and the cost of both the converter and filter [13]. Another benefit can be seen in reliability issues connected to the converter, as it can be seen as one of the most fragile components in the system, subject to both thermal and mechanical stresses [14], [15]. On the other hand, the reliability issue can be seen in the need for brushes in DFIG WECS, especially with the trend of increasing offshore wind energy penetration. In the alternative, the brushless DFIG can be used, but resulting in more windings, and higher leakage inductances [16].

As efficiency is the keyword in the green transition and the increased penetration of WECS is expected in future years, it is of the utmost importance to reduce the losses and weight of WECS. Wideband-gap devices, and in particular Silicon Carbide (SiC)-MOSFET devices, can viably be adopted to fulfill this goal. They have several advantages over Si devices, some of which are lower losses, higher temperature, and high-frequency operation suitable for a variety of applications [17], [18], [19], [20]. The higher voltage operation is enabled due to a much wider band gap than one of Si devices (3.3eV versus 1.1eV) and higher breakdown field (2.2mV/cm versus 0.3mV/cm) [21], [22]. Higher SiC thermal conductivity (theoretically 4.5W/cmK versus 2W/cmK) allows higher temperature operation as well as operation at higher current density ratings and reduction in the size of the cooling systems. The lower losses and higher efficiency of SiC are due to its higher band gap, higher breakdown field, and higher thermal conductivity. The high-frequency switching operation is enabled due to the higher electron velocity of SiC devices ($2x10^7$ cm/s versus $1x10^7$ cm/s). Besides, they require a smaller cooling system due to the higher efficiency and the ability to reduce the output filter size. All these factors can directly influence the levelized cost of energy (LCOE) of WECS.

Although SiC-MOSFETs have superior performance to Si-IGBTs, several distinct differences between the properties of SiC and Si materials and devices pose challenges to the robustness and reliability of SiC-MOSFETs [23], [24]. Particularly, the reliability issues refer to their ability to endure severe stress, both once and repeatedly. For instance, SiC MOSFETs have weaker short circuit (SC) robustness than their Si-IGBT counterparts, mainly due to their much smaller chip size and larger power density. Another reliability issue for SiC-MOSFETs is the gate oxide defects, especially in harsh operating conditions, since the gate oxides grown on SiC have a much higher density of defects than those grown on silicon. These defects eventually result in the degradation of static and dynamic characteristics in the case of repetitive SC and avalanche stress. Therefore, it is necessary to further improve the quality of the gate oxide of SiC MOSFETs. More generally, the assessment of SiC MOSFET reliability under application conditions still requires significant progress. Nonetheless, in the upcoming years, a significant market share for SiC MOSFET power devices in various applications is expected, along with cost reductions [25]. It is anticipated that by 2027, all major SiC power device manufacturers will have their own 200mm wafer SiC production facilities.

Many comparisons, including Si and SiC power devices for different kinds of WECS, have been made. When considering Type 4 WECS, in [26], the analysis with PMSG-based 10kW small-scale WECS is conducted, outlining the reduction in the volume of the passive components for the SiC-MOSFET-based system. Another work is considering the 1.5MW PMSG-based WECS, both Si- and SiC-based, and the comparison in terms of efficiency is provided [27]. Due to the differing ratings of IGBT and SiC devices, a fair comparison was not feasible. Also, in this case, the analysis lacked the cost comparison, while the volume was approximated for the two different converts. When considering Type 3 WECS, the analysis on the 2MW DFIG-based WECS has been conducted in [28], with a comparison of Si-, SiC-, and hybrid-based converters with different ratings, where the efficiency and volume were compared. This analysis lacked a comparison of the converter solutions cost.

The fair (considering devices/modules of the same power ratings) and complete (considering efficiency, volume, and cost) comparison was introduced in recently published papers [29], [30], [31] for SiC- and Si-based conversion systems in both Type 3 and 4 WECS. In [30], a detailed comparison between Si- and SiC-based WECS is presented for the full-scale PMSG-based systems. The analysis showed the significant reduction in the total volume in the SiC-based WECS when compared to Si-based WECS, while the cost was higher mainly due to the high SiC modules' cost. The

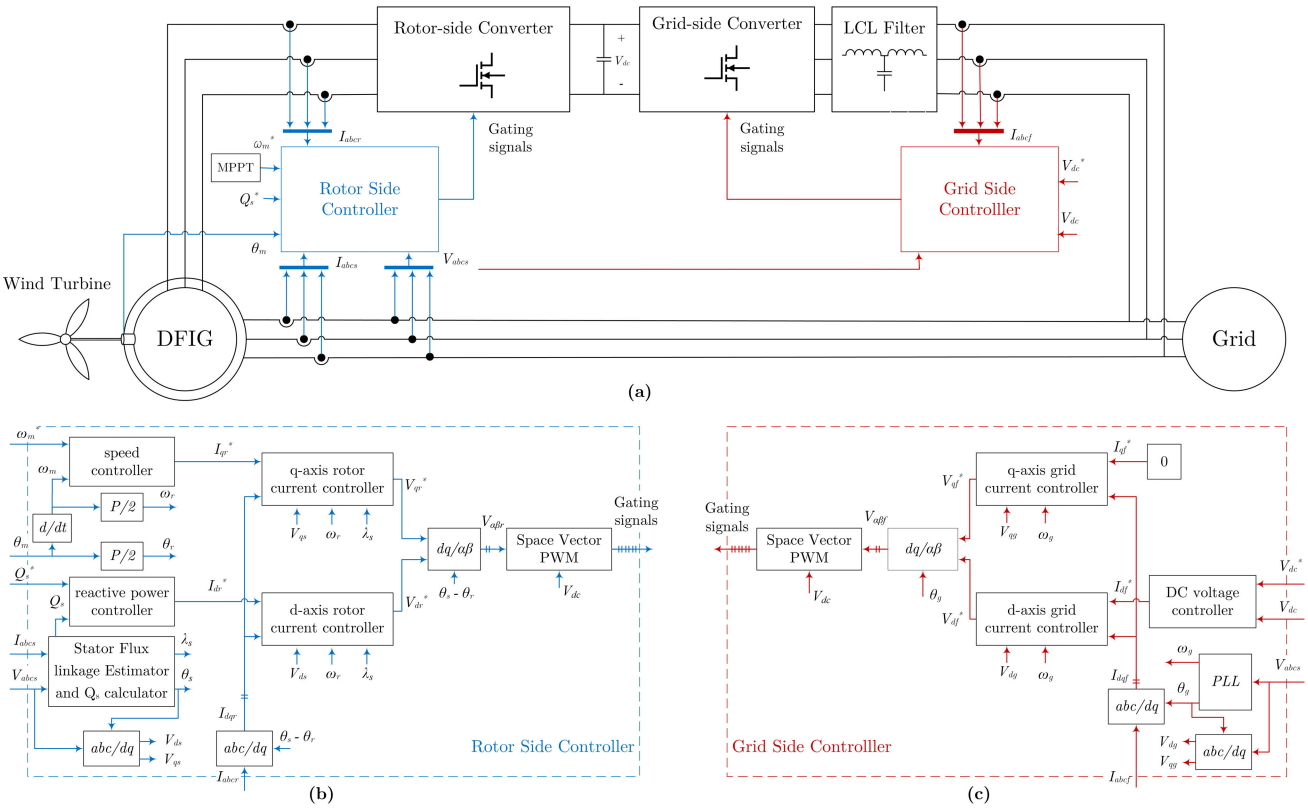

FIGURE 1. Block diagram of the DFIG-based WECS for the SiC-based converter solution: a) the whole system, b) RSC control, c) GSC control.

paper [31] is considering a 1.5 MW brushless doubly-fed reluctance generator (BDFRG) WECS with a bidirectional partial-scale frequency converter. Table 1 summarizes all the previously published literature related to Si- and SiC-based WECS comparisons.

Following a similar idea as in [31], this work is considering a 2 MW DFIG-based WECS with a partial-scale frequency converter comprised of two back-to-back power converters.

This paper's main contribution is to present a comprehensive and fair comparison of Si-IGBT and SiC-MOSFET-based converters in DIFG WECS, primarily in terms of efficiency and volume, and accordingly also the cost. This has been done using the complete simulation developed in the PLECS simulation tool, which comprises thermal analysis. The realistic libraries have been included for different power modules obtained from the manufacturers and based on the experimental data.

This paper is organized as follows: Section II presents a background regarding the DFIG-based wind turbine system, WECS modeling, control, converter, and filter modelling. Analysis of the efficiency and volume are presented in section III. Finally, simulation results for a 2MW WECS are presented in Section IV. The conclusions are given in Section V.

II. WECS MODELLING AND CONTROL

Typical Type 3 WECS is considered in this analysis, based on a DFIG, and a partial scale power converter is represented in Fig. I. The three-bladed horizontal axis wind turbine is connected to the shaft of the DFIG through a gear reducer. The DFIG has two sets of windings; the stator windings are connected directly to the grid, while the rotor windings are connected to the grid using brushes, a partial-scale back-to-back converter, and an LCL filter. Based on the current and voltage measurements and the shaft position sensor, the rotor-side converter (RSC) in Fig. 1b and grid-side converters (GSC) in Fig. 1c can be controlled to achieve maximum power point tracking (MPPT), control the power injected into

TABLE 1. Literature review on the comparison of the Si- and SiC-based WECS.

WECS type	Generator	Same Device Ratings	Compared Variables	Ref.
Type 4	PMSG/10 kW	No	Efficiency, cost, volume, and energy savings	[26]
Type 4	PMSG/1.5 MW	No	Efficiency, loss, and volume	[27]
Type 4	PMSG/2 MW	Yes	Efficiency and volume	[29]
Type 4	PMSG/2 MW	Yes	Efficiency, cost and volume	[30]
Type 3	DFIG/2 MW	No	Efficiency and volume	[28]
Type 3	BDFRG/1.5 MW	Yes	Efficiency, cost and volume	[31]

the grid, and control the DC bus voltage V_{dc}. This will be explained in more detail in the following section II-B.

A. DOUBLY-FED INDUCTION GENERATOR MODEL

To obtain the DFIG model in an arbitrary dq rotating reference frame, sinusoidally distributed three-phase windings on the stator and the rotor are assumed. The model could be derived using the winding function theory and Park transformation [32].

The stator quantities in the dq frame are transformed with an arbitrary angle $T(\theta)$, whereas the rotor quantities are obtained with an angle $T(\theta - \theta_r)$ using Park transformation. These rotor quantities are then referred to the stator side using the turns ratio.

The voltage equations in the arbitrary reference frame are given by:

$$v_{ds} = R_s i_{ds} + \frac{d\lambda_{ds}}{dt} - \omega\lambda_{qs} \tag{1}$$

$$v_{qs} = R_s i_{qs} + \frac{d\lambda_{qs}}{dt} + \omega\lambda_{ds} \tag{2}$$

$$v'_{dr} = R'_r i'_{dr} + \frac{d\lambda'_{dr}}{dt} - (\omega - \omega_r)\lambda'_{qr} \tag{3}$$

$$v'_{qr} = R'_r i'_{qr} + \frac{d\lambda'_{qr}}{dt} + (\omega - \omega_r)\lambda'_{dr} \tag{4}$$

where R_s and R'_r are the stator and rotor resistances in Ω, ω, and ω_r are the reference frame and the rotor electric angular speeds in rad/s. The equations above can represent the DFIG model in any reference frame. In this paper, the angle of the dq reference frame was selected to be the stator flux linkage angle θ_s, resulting in a rotating reference frame with a synchronous speed ω_s. Flux linkages are given by,

$$\lambda_{ds} = (L_{ls} + L_m)i_{ds} + L_m i'_{dr} \tag{5}$$

$$\lambda_{qs} = (L_{ls} + L_m)i_{qs} + L_m i'_{qr} \tag{6}$$

$$\lambda'_{dr} = (L'_{lr} + L_m)i'_{dr} + L_m i_{ds} \tag{7}$$

$$\lambda'_{qr} = (L'_{lr} + L_m)i'_{qr} + L_m i_{qs} \tag{8}$$

where the stator and rotor leakage inductances are denoted as L_{ls} and L'_{lr} respectively, both measured in H. The magnetizing inductance, also measured in H, is represented by L_m. The rotor parameters are indicated with a prime symbol to signify that they have been referred to the stator using the turns ratio a,

$$a = \frac{N_s}{N_r} \tag{9}$$

where the stator windings have N_s turns, and the rotor windings have N_r turns. The mechanical model is expressed as:

$$T_e = \frac{3}{2}\frac{P}{2}\left(\lambda'_{dr} i'_{qr} - \lambda'_{qr} i'_{dr}\right) \tag{10}$$

$$J\frac{d\omega_m}{dt} + B\omega_m = T_e - T_m \tag{11}$$

$$\omega_r = \frac{P}{2}\omega_m \tag{12}$$

where T_e and T_m are electromagnetic and mechanical torque in $N.m$, P is the number of poles, J is the equivalent moment of inertia in $kg.m^2$, and B is the damping coefficient in $kg.m^2/s$.

The main generator, turbine, and other parameters relevant to the system are presented in Table 2.

TABLE 2. Generator and system parameters.

Generator Parameters	
Rated power (MW)	2
Stator voltage (V)	690
Supply frequency (Hz)	50
Stator resistance (mΩ)	2.38
Rotor resistance (mΩ)	2.38
Stator leakage inductance (mH)	0.075
Rotor leakage inductance (mH)	0.06
Magnetizing inductance (mH)	2.273
Poles	4
Rated speed (rpm)	2000
Turbine Parameters	
Rotor diameter (m)	82
Hub height (m)	78–108
Cut-in wind speed (m/s)	2.5
Cut-out wind speed (m/s)	28–34
Rated wind speed (m/s)	12
Other Parameters	
DC-link voltage (V)	1200
Grid line-to-line voltage (V)	690

B. CONTROLLER AND CONVERTER MODELLING

In general, the reference frame could be selected as the stationary frame, the rotor frame, or the synchronous frame aligned with either the stator voltage or the stator flux. In this paper, the DFIG control system was implemented in a synchronous reference frame rotating and aligned with the stator flux linkage. In this case, the torque produced is proportional to the q-axis current, whereas the d-axis current is used for regulating reactive power. As a result, the control decoupling between the active power and reactive power can be realized [33].

When it comes to the RSC, a stator flux linkage estimator is used to obtain the stator flux linkage angle θ_s, which will be used to transform the stator quantities to the dq frame. The rotor quantities will be transformed using the angle $\theta_s - \theta_r$, where θ_r is the rotor electrical angle. A cascaded control structure is used with an outer speed/reactive power loop and an inner dq current loop. To achieve MPPT, the rotational speed of the generator must be controlled as,

$$\omega_m^* = \frac{V_w \lambda_{opt} N}{R} \tag{13}$$

where V_w is the wind speed, λ_{opt} is the optimal tip-speed ratio, N is the gear ratio, and R is the radius of the wind turbine. For both control loops, two-degrees-of-freedom PI (2DOF)

controllers are implemented [34] as:

$$I_{qr}^{*} = k_{p2\omega}\omega_{m}^{*} + k_{i\omega}\int(\omega_{m}^{*} - \omega_{m})\,dt - k_{p1\omega}\omega_{m} \tag{14}$$

$$I_{dr}^{*} = k_{p2Q}Q_{s}^{*} + k_{iQ}\int(Q_{s}^{*} - Q_{s})\,dt - k_{p1Q}Q_{s} \tag{15}$$

$$\begin{aligned} V_{qr}^{*} &= k_{p2q}I_{qr}^{*} + k_{iq}\int(I_{qr}^{*} - I_{qr})\,dt - k_{p1q}I_{qr} \\ &\quad + (\omega_{s} - \omega_{r})\sigma L_{r}I_{dr} + \frac{L_{m}}{L_{s}}V_{qs} - \omega_{r}\frac{L_{m}}{L_{s}}\lambda_{s} \end{aligned} \tag{16}$$

$$\begin{aligned} V_{dr}^{*} &= k_{p2d}I_{dr}^{*} + k_{id}\int(I_{dr}^{*} - I_{dr})\,dt - k_{p1d}I_{dr} \\ &\quad - (\omega_{s} - \omega_{r})\sigma L_{r}I_{qr} + \frac{L_{m}}{L_{s}}V_{ds} - \frac{L_{m}R_{s}}{L_{s}^{2}}\lambda_{s} \end{aligned} \tag{17}$$

where Q_s is the reactive power and σ is the leakage coefficient given by $1-L_m^2/(L_sL_r)$. Moreover, a limiter with anti-windup is implemented for each controller.

Space vector pulse width modulation (SVPWM) is finally used to obtain the gating signals from the reference voltages obtained from the current controllers [35].

On the grid-side controller, a phased-locked-loop (PLL) is used to obtain the grid angle θ_g from the measured voltages. The grid angle θ_g is used to transform the currents to the dq frame. Again, a cascaded control is implemented with an outer DC bus control loop and an inner current loop based on 2DOF PI controllers as:

$$I_{df}^{*} = k_{p2dc}V_{dc}^{*} + k_{idc}\int(V_{dc}^{*} - V_{dc})\,dt - k_{p1dc}V_{dc} \tag{18}$$

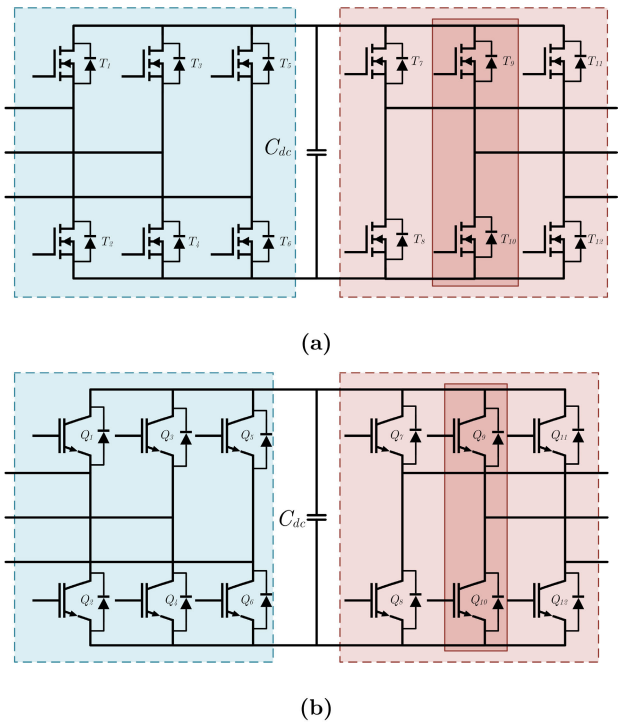

FIGURE 2. Back-to-Back converter topology: a) SiC-MOSFET with 6 half-bridge modules CAB650M17HM3, b) Si-IGBT with 6 half-bridge modules FF650R17IE4P.

TABLE 3. Module parameters.

SiC HB module parameters (CAB650M17HM3)	
Drain-source voltage V_{ds}	1700V
DC cont. drain current I_{ds} (@25 °C)	916A
DC cont. drain currentI_{ds} (@90 °C)	694A
Drain-Source On-State Resistance $R_{DS(on)}$ (@175 °C)	3.26 mΩ
Total gate charge Q_g	2988nC@V_{gs}= -4/15V
Gate-Source Voltage, Recommended V_{gs}	V_{gs}= -4/15V
Max junction temperature T_j	175 °C
Recommended min external gate on-resistance R_{g_on} (min)	1.5 Ω
Recommended min external gate off-resistance R_{g_off} (min)	1.5 Ω
Turn-on energy loss per pulse E_{on}(@125 °C)	44mJ(I_d=650A/V_{dd}=900V)
Turn-off energy loss per pulse E_{off}(@125 °C)	26mJ(I_d=650A/V_{dd}=900V)
IGBT HB module parameters (FF650R17IE4P)	
Collector-emitter voltage V_{ces}	1700V
Continuous DC collector current I_c (@175 °C)	650A
Total gate charge Q_g	7μC@V_{gs}=-15/15V
Gate-Emitter Voltage, Recommended V_{ge}	V_{ge}= -15/15V
Max junction temperature T_j	175 °C
Recommended min external gate on-resistance R_{g_on} (min)	1.8 Ω
Recommended min external gate off-resistance R_{g_off} (min)	2.7 Ω
Turn-on energy loss per pulse E_{on}(@125 °C)	300mJ(I_c=650A/V_{ce}=900V)
Turn-off energy loss per pulse E_{off}(@125 °C)	205mJ(I_c=650A/V_{ce}=900V)

$$\begin{aligned} V_{df}^{*} &= k_{p2f}I_{df}^{*} + k_{if}\int(I_{df}^{*} - I_{df})\,dt - k_{p1f}I_{df} \\ &\quad + V_{dg} - \omega_{g}L_{i}I_{qf} \end{aligned} \tag{19}$$

$$\begin{aligned} V_{qf}^{*} &= k_{p2f}I_{qf}^{*} + k_{if}\int(I_{qf}^{*} - I_{qf})\,dt - k_{p1f}I_{qf} \\ &\quad + V_{qg} + \omega_{g}L_{i}I_{df} \end{aligned} \tag{20}$$

where ω_g is the grid frequency and L_i is the inverter side filter inductance.

Also, in this case, SVPWM is used to obtain the gating signals from the commanded voltages obtained from the current controllers.

In DFIG WECS, a partial-scale converter is required in order to control the power at the generator output, because only a portion of the power passes through the converter. The half-bridge modules have been selected with the same ratings (1700V, 650A) for SiC-MOSFET and Si-IGBT converter, i.e., SiC-MOSFET module CAB650M17HM3 (Wolfspeed) and Si-IGBT module FF650R17IE4P (Infineon). The main parameters are shown in Table 3. Both for the rectifier and inverter stage, three of the half-bridge modules are connected to create a 2-level 3-phase inverter.

The current flowing through the devices is divided between the diode and the SiC-MOSFET/IGBT, depending on the polarity of the current. To meet the current rating of the system, it was sufficient to choose a single back-to-back converter: having the turbine current of 438 A_{rms} at nominal wind speed and grid-side current of 410 A_{rms}. Fig. 2 shows the 2-level 3-phase converters under consideration. In this paper, the SiC-MOSFET and Si-IGBT converters will be

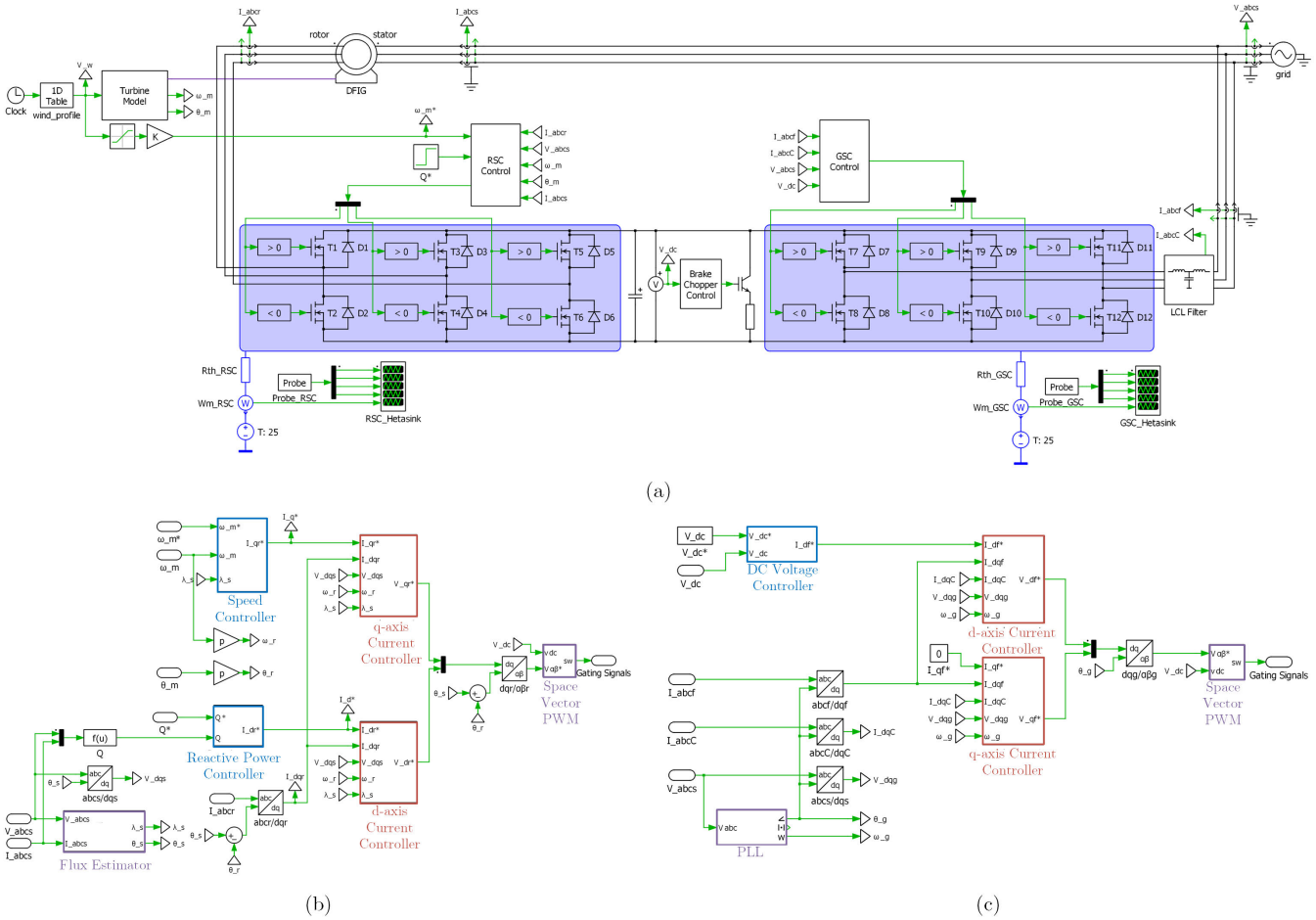

FIGURE 3. Details of the DFIG-based WECS implementation in PLECS for the SiC-based converter solution: a) the whole system, b) RSC control, c) GSC control.

investigated with the same control structure and compared in terms of efficiency, cost, and volume.

C. FILTER MODELLING

An LCL-type filter was chosen because it is smaller and provides higher attenuation compared to an L-type filter. However, the downside of using an LCL filter is that it requires passive or active damping to operate stably, which may make the system more complex. The LCL filter is composed of an inverter-side inductor L_i, a grid-side inductor L_g, and a capacitor C_f.

The LCL filter is designed as follows: first, the inverter-side inductor L_i is selected based on the desired current ripple and the switching frequency as [36]:

$$L_i = \frac{2}{3}\frac{V_{dc}}{\Delta I_g f_{sw}}(1-m)m \tag{21}$$

where ΔI_g is the desired current ripple, V_{dc} is the DC bus voltage, f_{sw} is the switching frequency, and m is the modulation index. The grid-side inductor, L_g, is chosen as a proportion of L_i.

$$L_g = rL_i \tag{22}$$

where r is the ratio and is selected as 15%.

Finally, to ensure the reduction of total harmonic distortion (THD), the selection of the filter capacitor is made using:

$$C_f = \frac{1}{L_g(2\pi f_{sw})^2 \frac{THD}{K_{i\%}}} \tag{23}$$

where $K_{i\%}$ is the desired percentage of current ripple $K_{i\%} = \Delta I_g / I_{g(peak)}$. Using the above design procedure, the LCL filter parameters for a switching frequency of 5kHz and 40kHz are shown in Table 4.

TABLE 4. Filter parameters.

Switching frequency	5 kHz	40 kHz
Inverter-side inductor L_i (μH)	281.6	35.2
Grid-side inductor L_g (μH)	42.2	5.28
Capacitor C_f (μF)	120	15

III. EFFICIENCY, LOSSES AND VOLUME ANALYSIS

The complete DFIG WECS has been built in a PLECS simulation tool, as in Fig.3, for the case of the SiC-MOSFET-based converter. The details on the RSC and GSC control

are given in Figs. 3b and 3c, respectively. The DFIG block was modeled based on equations (1)-(12), while the controllers were implemented based on equations (14)-(20). The DFIG WECS for the case of Si-IGBT-based converter is analogue, only the SiC-MOSFETs are replaced with Si-IGBT modules.

PLECS is a convenient simulation tool, as it allows the user to merge the electrical and thermal design. Effectively, it has the capability to simulate the electrical, loss, and thermal characteristics based on the specified condition of the converters and power devices. The thermal behavior of the converter modelled with the PLECS simulation tool and based on the manufacturer's libraries for a specific device/module demonstrates the strong alignment with the experimental results [37].

In further analysis, for the efficiency and losses, only the converter losses have been considered, as the other losses are similar for the SiC-MOSFET and Si-IGBT-based WECS. For the volume, instead, the filter volume and heat sink volume are taken into account, as these are the only aspects that exhibit variance between the two systems.

A. CONVERTER LOSSES

The libraries provided by the modules' manufacturers allow the thermal description of the devices to be inserted in the PLECS. The library includes the switching and conduction losses (based on the different external gate resistances R_{g_on} and R_{g_off}) and the parameters for the Cauer or Foster thermal network. Note that Foster and Cauer models are equivalent representations of the device's thermal behavior, but Cauer models are more representative of the physical structure of the device. The switching and conduction losses of the modules are inserted for each operating condition (forward current, blocking voltage, and junction temperature) in terms of 3D look-up tables and have been verified experimentally by the manufacturer in the standard double pulse-testing setup and with acceptable accuracy for the power loss calculation [37], [38]. Both thermal models and losses are not visible in Fig. 3, but are included inside each device as a separate library.

Example of the SiC-MOSFET's base on-energy E_b is given in the Fig. 4. This energy is afterward used to calculate the switching energy during the turn-on processes in the case of different external on-gate resistances R_{g_on} by the following equation (provided by the manufacturer):

$$E_{on} = E_b(-0.62834\, R_{g\_on}^2 + 16.4425 R_{g\_on} + 30.1859)/53.4359 \quad (24)$$

A similar equation can also be found for the turn-off losses. The same procedure is also applied to the Si-IGBT module. The minimum external gate resistances recommended by manufacturers have been selected for the analysis (Table 3), as they allow switching loss minimization. A Cauer thermal network has been utilized for the thermal description of the SiC-MOSFET modules, while for Si-IGBT the Foster network parameters were provided.

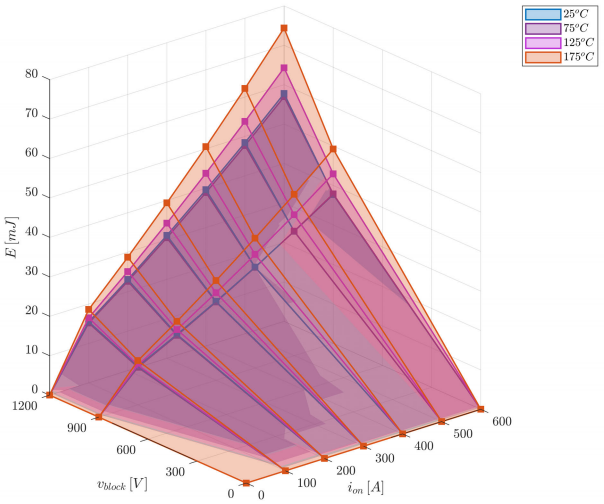

FIGURE 4. Example of SiC-MOSFET module base-switching energy during the turn-on (E_b) for different temperatures.

After the loss description was added in PLECS and the thermal network was created for each converter, it was possible to select the appropriate heat sink. In this way, the respective converter losses, together with the junction and heat sink temperature, can be measured. In Fig. 3, the heatsink is represented in light blue color, while the losses were taken with the heat flow meter.

B. VOLUME ANALYSIS

The heat sink volume analysis was based on the results coming from the power loss analysis of the two converters (with both SiC-MOSFET and Si-IGBT modules) for a range of switching frequencies (3kHz-40kHz for SiC-MOSFET and 1kHz-5kHz for Si-IGBT) and at a nominal wind speed of 12 m/s, considering a 70 °C heat sink temperature, and 25 °C and 55 °C of the ambient temperature. The 70 °C heat sink temperature has been chosen in order to keep the junction temperature below the maximum value, and the 55 °C ambient temperature is representative of really hot climates such as tropical.

In order to evaluate the heat sink volume, it is necessary to calculate its thermal resistance:

$$r_h = \frac{T_h - T_a}{P_{tloss}} \quad (25)$$

where T_h is the heat sink temperature, T_a is the ambient temperature, and P_{tloss} is the total converter loss. Once r_h is calculated, it is possible to choose the right heat sink and obtain its volume. As the thermal resistances resulted in a very low value for the range of switching frequencies (i.e., from 0.004 °C/W - 0.02°C/W), active liquid cooling was the only possible choice [39].

Five different cold plates have been analyzed from three different manufacturers, as shown in Fig. 5, both with 4-pass (for higher thermal resistances) and 6-pass tubes (for lower thermal resistances). As the volumes were rather similar in Fig. 5a, also the cost analysis has been conducted, as shown

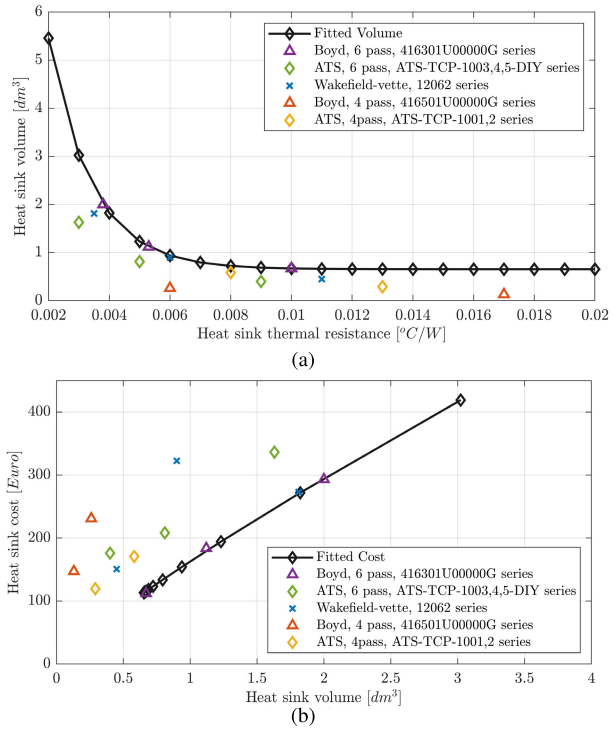

FIGURE 5. Liquid cold plate heat sinks from different manufacturers: a) volume, b) cost.

in Fig. 5b. The heat sink with the lowest cost has been selected for further analysis, i.e., Boyd 6-pass tube (in violet color). Only the volume of the liquid cold plate has been considered for the volume analysis, excluding the volume of other components, such as the pump and heat exchanger, as it is the same for all the heat sinks. For the selected heat sink, the curve fitting has been done to obtain the volume equation:

$$vol_h = 0,6531151 + 19,72284e^{(-706,3113r_h)} \tag{26}$$

where vol_h is expressed in dm^3 and r_h in °C/W.

The curve-fitted data presented in Fig. 5 will be utilized in the results section to estimate the heat sink cost and volume for any thermal resistance.

The volume of the filter's parameters was calculated based on the method presented in [40]:

$$vol_L = k_L A_p^{3/4} \tag{27}$$

where the area product A_p is defined as the product of the core window winding area and the cross-sectional area, and k_L is the inductor coefficient. Area product A_p can be obtained by the following equation:

$$A_p = \left[\frac{\sqrt{1+\gamma}K_i L\hat{I}^2}{B_{max}K_t\sqrt{k_u\Delta T}}\right]^{8/7} \tag{28}$$

where γ is defined to be the core loss as a fraction of the winding loss and is assumed to be 0.03 [41], B_{max} is the maximum flux density and is dependent on the switching frequency, K_i is the current waveform factor, K_t is 48.2×10^3 (according to [40]), $\hat{I}$ is the peak value of current, and k_u is the window utilization factor defined as the ratio of the total conduction area to the total window winding area of the core. A maximum temperature rise ΔT of 60°C is chosen to maintain high current density in the windings and stay within recommended operating temperature limits for the core. It is evident from these equations that the volume of the inductor is proportional to the inductance value. The capacitor volume could be calculated using [41],

$$vol_C = k_c C_f V_{nom} \tag{29}$$

where V_{nom} is the nominal voltage and k_c is the capacitor coefficient.

IV. RESULTS AND DISCUSSION

In this section, the analyses were conducted comparing the efficiency, volume, and cost of two wind conversion systems based on SiC-MOSFET and Si-IGBT.

Fig. 6 shows the efficiency of the two conversion systems in the case of different switching frequencies, considering both RSC and GSC, as presented in Fig.3. In particular, the minimum value for the gate on and off resistances are considered for the SiC-MOSFET-based converter ($R_{g\_on} = 1.5\Omega$, $R_{g\_off} = 1.5\Omega$) and for a Si-IGBT-based converter ($R_{g\_on} = 1.8\Omega$, $R_{g\_off} = 2.7\Omega$). The heat sink temperature was 70 °C for all cases. The nominal wind speed of 12m/s was taken into account.

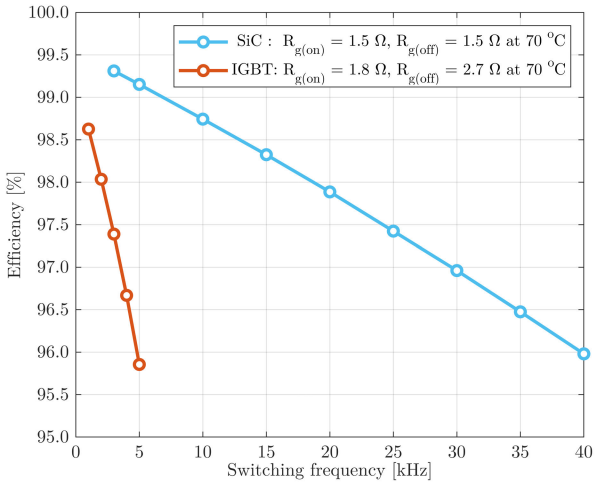

FIGURE 6. Efficiency for the two WECSs at full power rating at defined switching frequency range.

The choice for the switching frequency range was made to ensure that only practical and realistic conditions were considered for both WECS. As for the low switching frequencies (3 and 5kHz), the SiC-MOSFET-based converter shows higher efficiency, which is 3% higher in the case of 5kHz. For the optimal switching frequency for both converters (40kHz for SiC-MOSFET and 5kHz for Si-IGBT converter), the efficiency is rather similar. For this case, the losses in the SiC MOSFET converter are mainly switching

losses, as conduction losses are very low (17.4kW or 3.2% of the rated converter power for switching and 3.2kW or 0.6% of the rated converter power for conduction losses for both RSC and GSC). Similarly, for the Si IGBT, the total conduction losses are 4.3kW or 0.8% of the rated converter power, and the switching losses are 16.8kW or 3.17% of the rated converter power. The real benefit of the material properties of the SiC-based converter can be seen when it is subjected to the same conditions as the Si-based converter, i.e., a 5kHz switching frequency. In this scenario, the SiC MOSFET-based converter has 2.3kW conduction losses and 1.8kW switching losses, showing a significant difference in both conduction and switching losses compared to the Si IGBT converter.

The optimal switching frequency for both systems was selected based on electrical and thermal requirements, considering the safe operating area and recommendations of power modules, maximum modules' junction temperatures, and maximum heat sink temperature, allowing the thermal resistance to still be feasible for the liquid cooling-based heat sinks. The maximum switching frequency is selected in order to have a reduction in the output filter volume.

Regarding the volume analysis, Fig. 7 illustrates the specific volumes of passive components. It delineates the volumes of grid-side and inverter-side inductors, capacitor volume, and the overall filter volume (depicted in the red trace) in Fig. 7a. Fig. 7b presents the heat sink volumes for the SiC-MOSFET-based converter (in red and light blue traces) and the heat sink volumes for the Si-IGBT-based converter (in green and yellow traces) under ambient temperatures of 25 °C and 55 °C.

In terms of the filter volume, it's evident that the inverter-side inductor stands out as the largest component within the filter, as indicated by the yellow trace in Fig. 7a. The volume occupied by the capacitor is negligible when compared to the other components. The overall filter volume tends to decrease as the switching frequency increases. However, this pattern does not hold for the heat sink volume, which increases with higher switching frequencies. When considering the different ambient temperatures, i.e., 25 °C and 55 °C, the heat sink volume at 55 °C is 3.3 times higher than the one at 25 °C. The total filter volume is much higher than the heat sink volume, justifying in this way the fact that the maximum possible switching frequencies were considered for the optimal case.

At the optimal switching frequencies (specifically, 40kHz for the SiC-MOSFET-based converter and 5kHz for the Si-IGBT-based converter), the heat sink volumes appear to be quite similar. This observation aligns with the information presented in Fig. 6, where the efficiencies for these particular frequencies also demonstrate similarity.

For further analysis, the following parameters have been considered for the comparison: the minimum required on and off external gate resistances for both the conversion systems as in Table 3 and the heat sink temperature of 70 °C. The wind speed was variable. The power factor was kept at 0.95, staying

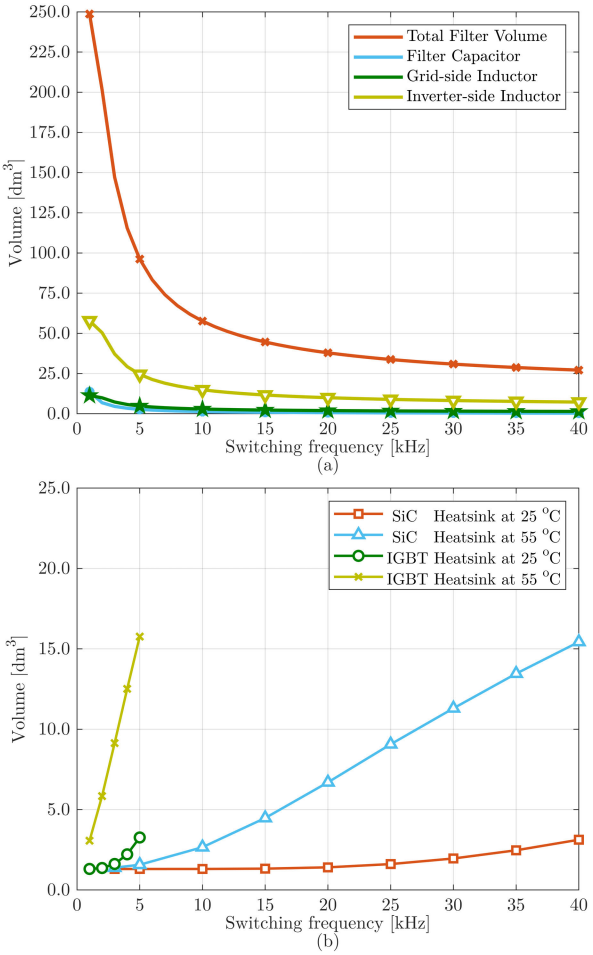

FIGURE 7. Different passive components volumes for different switching frequencies: a) filter volume, b) heat sink volume.

within the power factor range usually defined for minimum reactive power control. For selected frequencies, including the optimal ones, Fig. 8 shows the efficiency, converter power, and THD of the output converter current comparison for different wind speeds, considering 5, 35, and 40kHz switching frequencies for the SiC-MOSFET-based converter (blue and red traces) and 3 and 5kHz for the Si-IGBT-based converter (gray traces). Both sub-synchronous and super-synchronous modes were taken into account. The rotor power is negative for the sub-synchronous mode, meaning that the power is absorbed by the rotor (for lower wind speeds), and positive for the super-synchronous mode, where the power is delivered to the grid (for the wind speeds greater than 9m/s). As for the efficiency, the zero efficiency associated with the zero rotor power at synchronous speed has been omitted for readability reasons. SiC-MOSFET at 5kHz clearly has the highest efficiency. The lowest efficiency is seen for the SiC-MOSFET converter with the highest switching frequency. When considering Si-IGBT at 5kHz, we can note similar efficiency as the one of SiC-MOSFET at 40kHz, slightly higher for lower wind speeds and practically the same for 10 and 12m/s. There is a big difference in the

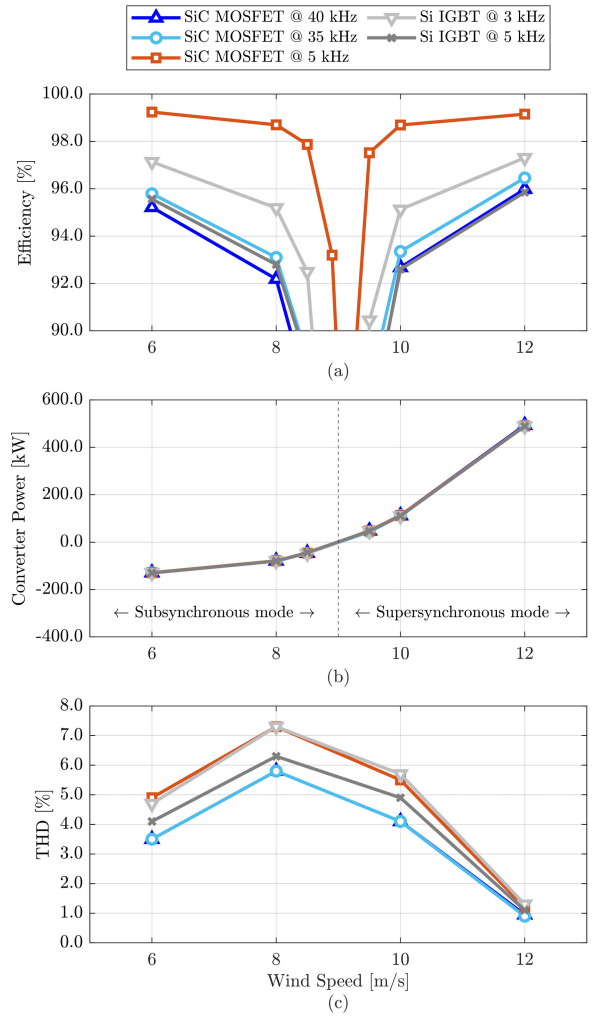

FIGURE 8. Comparison of SiC-MOSFET- and Si-IGBT-based converters for different wind speeds and selected switching frequencies: a) efficiency, b) converter power, c) THD of the output converter current.

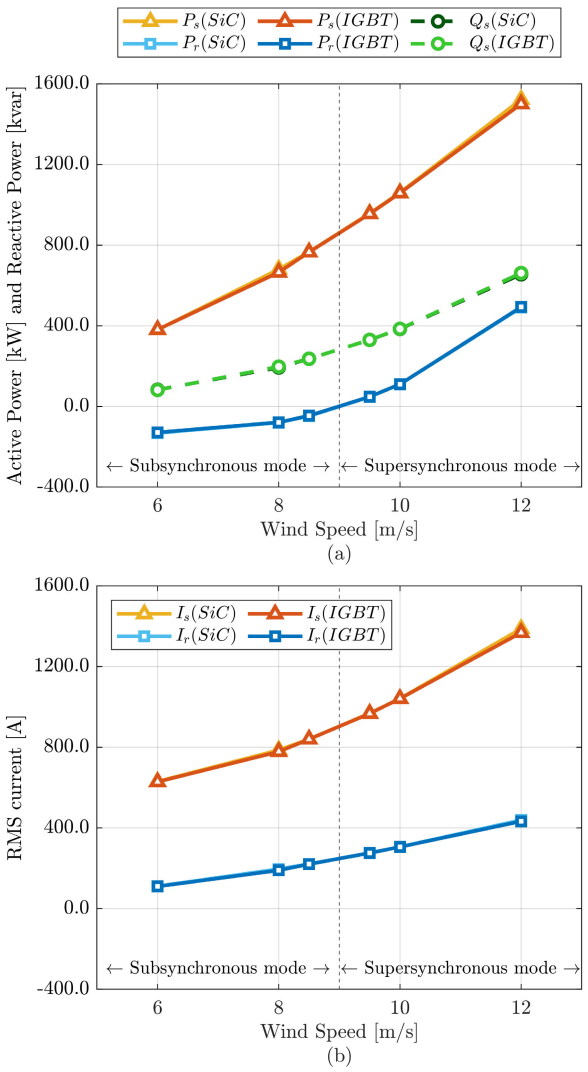

FIGURE 9. Stator and rotor power and currents for SiC-MOSFET- and Si-IGBT-based WECS for different wind speeds: a) powers, b) currents.

efficiency when looking at the Si-IGBT at 3 and 5kHz, with the highest difference of 2.52% at 10m/s. For this reason, it is important to have the overall picture, comparing the volume and cost in order to decide for the best working condition or the optimal solution. As for the converter power, we can see that for the power, all the cases show similar power flow. The power does not increase linearly with wind speed; instead, there is a lower power output for wind speeds of 8 and 10 m/s compared to 6 m/s when looking at the absolute values, for example. This is due to the fact that the rotor power P_r is related to the stator power P_s and the mechanical power P_m by [32]:

$$P_r = -sP_s = -\frac{s}{1-s}P_m \tag{30}$$

where s is the slip. As the wind speed changes, the optimal rotor speed for MPPT changes, which in turn varies the slip and, thus, the rotor power.

For the THD of the output current instead, the highest values are reached for the lowest switching frequencies, i.e., 3kHz and 8m/s wind speed, while the lowest values are for the SiC-MOSFET with 40kHz. However, all THD is far below the limit of 5% required for the grid connection at nominal wind speed.

Fig. 9 shows the simulation results for the stator and rotor active power, stator reactive power, and stator and rotor current for both Si-IGBT and SiC-MOSFET based systems at different wind speeds. The rotor reactive power is zero due to applied control. Namely, from the figure, the same behavior of powers and currents can be noted for both Si- and SiC- based systems. Both the stator power and rotor power increase with wind speed, but at different rates, as explained previously in eq. (30). For instance, in the case of 12m/s wind speed, the slip is -33.33%, and the rotor power is 1/3 the stator power. In other cases, the slip is positive for speeds below the synchronous speeds (sub-synchronous mode) and negative for speeds above the synchronous speed (super-synchronous mode). The slip has a greater magnitude for the wind speed of 6m/s and lower for the 8m/s and 10m/s, witnessed by the higher difference in the powers for these cases.

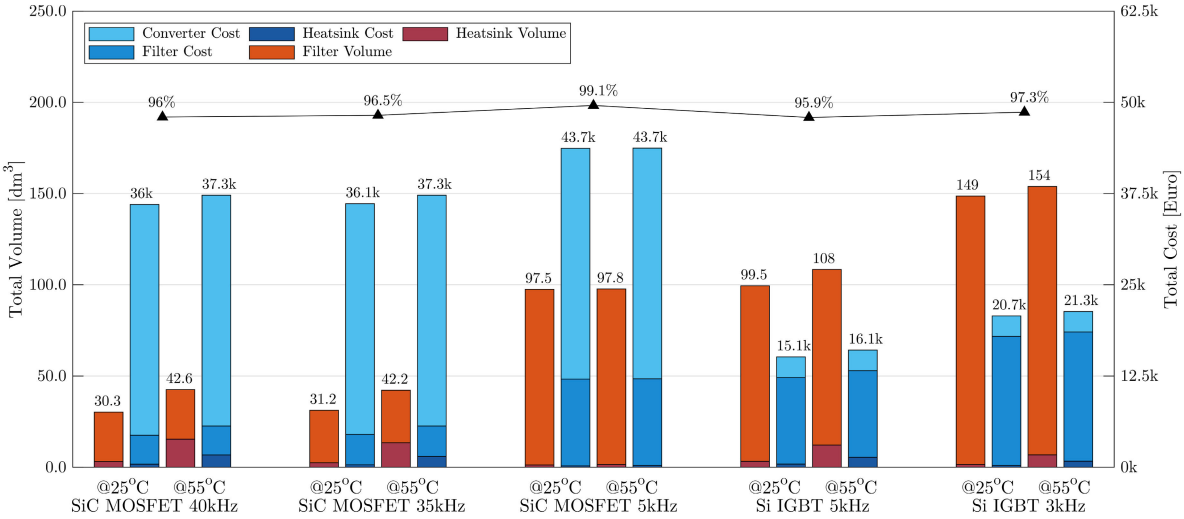

FIGURE 10. Comparison of SiC-MOSFET- and Si-IGBT-based converters for different ambient temperatures and selected switching frequencies: efficiency, volume, and cost.

Fig. 10 summarizes the volume comparison (in dm^3, including the filter and heat sink volume) and a cost comparison of the converter, filter, and heat sink (in Euros) for the selected switching frequencies and nominal wind speed.

The efficiency of various cases has also been included to enhance readability, particularly for the nominal wind speed for which the system has been designed in terms of heat sink and filter.

For the cost of the heat sink, the one with the lowest cost has been considered, as in Fig. 5b. This cost has then been fitted in order to obtain the cost for different volumes resulted from the analysis:

$$cost_h = 162,782 \times vol_h^{0,8547905} \tag{31}$$

where vol_h is expressed in dm^3 and $cost_h$ in Euro. A similar procedure has also been done for the filter cost. Information on the different filters' costs available in [42] has been used to obtain the curve fitting:

$$cost_f = 114.5 \times vol_f + 857.2 \tag{32}$$

where $cost_f$ is expressed in euros and the volumes vol_f in dm^3.

The volume is represented in orange and brown color in Fig. 10. In all cases, the heat sink volume is much lower than the filter volume. The SiC-MOSFET-based converter with a 40kHz switching frequency has the lowest total volume, 3.2 times lower (2.3 times in the case of 55 °C ambient temperature) when compared to a SiC-MOSFET-based converter at 5kHz, and 4.9 times (3.62 in the case of 55 °C ambient temperature) when compared to the Si-IGBT-based converter at 3kHz. Instead, when compared to Si-IGBT at 5kHz, the volume is 3.3 times lower (2.53 times for 55 °C ambient temperature).

Again, when looking at the different costs represented in blue, the heat sink cost is almost negligible compared to the cost of the filter and converter. The dominant cost in SiC-MOSFET based WECS is the converter cost, while for the Si-IGBT based WECS, it is the filter cost. The highest cost in the SiC-MOSFET-based converter is the converter cost, which is 11.3 times higher when compared to the Si-IGBT-based converter. The filter cost, instead, at 40kHz, is 4.5 times lower than the one at 3kHz and 3 times lower than the one at 5kHz.

When considering the SiC-MOSFET-based converter at 5kHz, the only benefit can be seen in the efficiency, as it is the highest one, i.e. 99.1%. It has the highest cost due to the high converter cost but also the filter cost, as the switching frequency is low. As for the volume, it is comparable to the one of Si-IGBT at the same switching frequency.

Ruling out all the cases that clearly do not represent the most optimal candidate and focusing solely on the optimal working conditions of the two converters (specifically, 5kHz for the Si-IGBT-based converter and 40kHz for the SiC-MOSFET-based converter), it's apparent that, despite similar converter efficiency at the nominal wind speed of 12 m/s (95.9% and 96%, respectively), the SiC-MOSFET-based converter demonstrates a 3.3 times lower total volume compared to the Si-IGBT-based converter. However, the total cost, comprising the converter, filter, and heat sink, is more than 2 times higher for the SiC-MOSFET-based converter. This is primarily attributed to the elevated module cost associated with the SiC-MOSFET based WECS. This situation can change with the decrease in the price of Silicon Carbide-based power devices. In fact, the 50% decrease in the price would make the SiC-MOSFET modules the absolute best choice in DFIG WECS.

V. CONCLUSION AND FUTURE WORK

A 2 MW DFIG-based Wind Energy Conversion System with a bidirectional partial-scale frequency converter composed of two back-to-back converters is considered for this analysis, and an efficiency, volume, and cost fair comparison for

Si- and SiC-based converters was conducted, previously not presented in the available literature. Simulations using realistic thermal models for the power modules have concluded that employing SiC-based converters in the wind generation system will achieve efficiency comparable to Si-based converters while also reducing the overall system size. Particularly, a reduction of 3.3 times in the total volume necessary for the passive components was observed. This was not the case with the price, which showed that the SiC-based system was twice as costly as the one in Si. With the price reduction in SiC-based power devices, the benefits of this system will be more marked, as the filter cost is much lower in this case. In particular, with the price reduction of 50%, SiC-MOSFET modules would be the absolute best choice in DFIG WECS.

For future work, the authors plan to conduct a similar analysis using the Hardware in the Loop (HIL) system. In addition to achieving results that closely match those measured on the real WECS, this approach is expected to yield two significant benefits: first, it will allow for verification of both the correctness of the approach and the applied control methods; second, it will enable a comparison between the HIL and PLECS results. Moreover, the work can be expanded by conducting comparative studies with different multilevel converter topologies, which allow the utilization of switches with lower voltage ratings, as well as exploring advanced control techniques suitable for improving the reliability of SiC-MOSFETs.

REFERENCES

[1] V. Yaramasu, B. Wu, P. C. Sen, S. Kouro, and M. Narimani, "High-power wind energy conversion systems: State-of-the-art and emerging technologies," *Proc. IEEE*, vol. 103, no. 5, pp. 740–788, May 2015.

[2] R. L. Iglesias, R. L. Arantegui, and M. A. Alonso, "Power electronics evolution in wind turbines—A market-based analysis," *Renew. Sustain. Energy Rev.*, vol. 15, no. 9, pp. 4982–4993, Dec. 2011.

[3] O. Anaya-Lara, N. Jenkins, J. B. Ekanayake, P. Cartwright, and M. Hughes, *Wind Energy Generation: Modelling and Control*. Hoboken, NJ, USA: Wiley, 2011.

[4] Y. Zhou, P. Bauer, J. A. Ferreira, and J. Pierik, "Operation of grid-connected DFIG under unbalanced grid voltage condition," *IEEE Trans. Energy Convers.*, vol. 24, no. 1, pp. 240–246, Mar. 2009.

[5] H. J. Baesmat and M. Bodson, "Pole placement control for doubly-fed induction generators using compact representations in complex variables," *IEEE Trans. Energy Convers.*, vol. 34, no. 2, pp. 750–760, Jun. 2019.

[6] N. K. Mishra, Z. Husain, and A. Iqbal, "Modeling and analysis of novel six-phase DFIG through asymmetrical winding structure for disperse generation," *Int. Trans. Electr. Energy Syst.*, vol. 30, Sep. 2020, Art. no. e12649.

[7] T. Kawaguchi, T. Sakazaki, T. Isobe, and R. Shimada, "Offshore-wind-farm configuration using diode rectifier with MERS in current link topology," *IEEE Trans. Ind. Electron.*, vol. 60, no. 7, pp. 2930–2937, Jul. 2013.

[8] S. Müller, M. Deicke, and R. W. De Doncker, "Doubly fed induction generator systems for wind turbines," *IEEE Ind. Appl. Mag.*, vol. 8, no. 3, pp. 26–33, Jun. 2002.

[9] M. Yamamoto and O. Motoyoshi, "Active and reactive power control for doubly-fed wound rotor induction generator," *IEEE Trans. Power Electron.*, vol. 6, no. 4, pp. 624–629, Oct. 1991.

[10] L. Xu and Y. Wang, "Dynamic modeling and control of DFIG-based wind turbines under unbalanced network conditions," *IEEE Trans. Power Syst.*, vol. 22, no. 1, pp. 314–323, Feb. 2007.

[11] M. Abulizi, W. Shi, Y. Hu, M. Bahati, and C. Zhang, "Study on current controller of doubly-fed induction generator with variable parameters," in *Proc. IEEE 4th Int. Conf. Power, Electron. Comput. Appl. (ICPECA)*, Shenyang, China, Jan. 2024, pp. 484–489.

[12] H. Polinder, F. F. A. Van Der Pijl, G.-J. De Vilder, and P. J. Tavner, "Comparison of direct-drive and geared generator concepts for wind turbines," *IEEE Trans. Energy Convers.*, vol. 21, no. 3, pp. 725–733, Sep. 2006.

[13] H. A. Hussain, "Optimal gearbox ratio to minimize the power converter ratings in DFIG-based type-3 wind turbines," *IEEE Access*, vol. 11, pp. 52158–52167, 2023.

[14] D. Zhou, G. Zhang, and F. Blaabjerg, "Optimal selection of power converter in DFIG wind turbine with enhanced system-level reliability," *IEEE Trans. Ind. Appl.*, vol. 54, no. 4, pp. 3637–3644, Jul. 2018.

[15] H. Cui, T. Guo, C. Yang, Y. Dai, C. Wang, H. Du, L. Qin, and H. Yu, "A new thermal management strategy of IGBT in DFIG for economic benefit maximization," *IEEE Trans. Ind. Informat.*, vol. 20, no. 2, pp. 1335–1347, Feb. 2024.

[16] O. I. Olubamiwa, T. Hutton, and N. Gule, "Brushless doubly fed machine design evaluation with power factor considerations," *IEEE Trans. Ind. Appl.*, vol. 59, no. 2, pp. 1457–1468, Mar. 2023.

[17] V. Joshi, U. Jadli, P. Pande, M. Chaturvedi, D. Haasmann, and S. Dimitrijev, "Circuit-specific and technology-independent criterion for selection of power MOSFETs that minimize energy dissipation," *IEEE Access*, vol. 11, pp. 116472–116479, 2023.

[18] H. Zhang and L. M. Tolbert, "SiC's potential impact on the design of wind generation system," in *Proc. 34th Annu. Conf. IEEE Ind. Electron.*, Nov. 2008, pp. 2231–2235.

[19] A. Hussein and A. Castellazzi, "Comprehensive design optimization of a wind power converter using SiC technology," in *Proc. Int. Conf. Smart Grid (icSmartGrid)*, Dec. 2018, pp. 34–38.

[20] T. Ilahi, T. Izhar, S. M. Qaisar, U. T. Shami, M. Zahid, A. Waqar, and A. Alzahrani, "Design and performance analysis of ultra-wide bandgap power devices-based EV fast charger using bi-directional power converters," *IEEE Access*, vol. 11, pp. 25285–25297, 2023.

[21] A. Kumar, M. Moradpour, M. Losito, W.-T. Franke, S. Ramasamy, R. Baccoli, and G. Gatto, "Wide band gap devices and their application in power electronics," *Energies*, vol. 15, no. 23, p. 9172, Dec. 2022.

[22] J. Millán, P. Godignon, X. Perpiñà, A. Pérez-Tomás, and J. Rebollo, "A survey of wide bandgap power semiconductor devices," *IEEE Trans. Power Electron.*, vol. 29, no. 5, pp. 2155–2163, May 2014.

[23] J. Wang and X. Jiang, "Review and analysis of SiC MOSFETs' ruggedness and reliability," *IET Power Electron.*, vol. 13, no. 3, pp. 445–455, Feb. 2020.

[24] R. Yu, S. Jahdi, O. Alatise, J. Ortiz-Gonzalez, S. P. Munagala, N. Simpson, and P. Mellor, "Measurements and review of failure mechanisms and reliability constraints of 4H-SiC power MOSFETs under short circuit events," *IEEE Trans. Device Mater. Rel.*, vol. 23, no. 4, pp. 544–563, Dec. 2023.

[25] M. Thoben and M. Pfost, "Application readiness map for WBG-semiconductor-based applications," in *Proc. 25th Eur. Conf. Power Electron. Appl. (EPE ECCE Europe)*, Aalborg, Denmark, Sep. 2023, pp. 1–7.

[26] A. Hussein, A. Castellazzi, P. Wheeler, and C. Klumpner, "Performance benchmark of Si IGBTs vs. SiC MOSFETs in small-scale wind energy conversion systems," in *Proc. IEEE Int. Power Electron. Motion Control Conf. (PEMC)*, Sep. 2016, pp. 963–968.

[27] H. Zhang and L. M. Tolbert, "Efficiency impact of silicon carbide power electronics for modern wind turbine full scale frequency converter," *IEEE Trans. Ind. Electron.*, vol. 58, no. 1, pp. 21–28, Jan. 2011.

[28] A. Arrizabalaga, A. Idarreta, M. Mazuela, I. Aizpuru, U. Iraola, J. L. Rodriguez, D. Labiano, and I. Alisar, "Impact of silicon carbide devices in 2 MW DFIG based wind energy system," in *Proc. 22nd Eur. Conf. Power Electron. Appl. (EPE ECCE Europe)*, Sep. 2020, pp. P.1–P.10.

[29] J. Loncarski, H. A. Hussain, and A. Bellini, "High-power SiC module in wind turbine full scale frequency converter: Efficiency comparison with IGBT-based converter," in *Proc. 2nd Int. Conf. Sustain. Mobility Appl., Renew. Technol. (SMART)*, Nov. 2022, pp. 1–7.

[30] J. Loncarski, H. A. Hussain, and A. Bellini, "Efficiency, cost, and volume comparison of SiC-based and IGBT-based full-scale converter in PMSG wind turbine," *Electronics*, vol. 12, no. 2, p. 385, Jan. 2023.

[31] J. Loncarski, H. A. Hussain, T. Taluo, and L. Ristic, "BDFRG based WECS with partial-scale converter: Efficiency, cost and volume comparison of SiC-based and IGBT-based converter solution," in *Proc. IEEE Belgrade PowerTech*, Belgrade, Serbia, Jun. 2023, pp. 1–6.
[32] G. Abad, J. Lopez, M. Rodriguez, L. Marroyo, and G. Iwanski, *Doubly Fed Induction Machine: Modeling and Control for Wind Energy Generation*. Hoboken, NJ, USA: Wiley, 2011.
[33] D. Xu, F. Blaabjerg, W. Chen, and N. Zhu, *Advanced Control of Doubly Fed Induction Generator for Wind Power Systems*. Hoboken, NJ, USA: Wiley, 2018.
[34] H. A. Hussain, "Tuning and performance evaluation of 2DOF PI current controllers for PMSM drives," *IEEE Trans. Transport. Electrific.*, vol. 7, no. 3, pp. 1401–1414, Sep. 2021, doi: 10.1109/TTE.2020.3043853.
[35] G. Holmes and T. A. Lipo, *Pulse Width Modulation for Power Converters: Principles and Practice*. Hoboken, NJ, USA: Wiley, 2003.
[36] A. Reznik, M. G. Simões, A. Al-Durra, and S. M. Muyeen, "*LCL* filter design and performance analysis for grid-interconnected systems," *IEEE Trans. Ind. Appl.*, vol. 50, no. 2, pp. 1225–1232, Mar. 2014.
[37] K. Ma, A. S. Bahman, S. Beczkowski, and F. Blaabjerg, "Complete loss and thermal model of power semiconductors including device rating information," *IEEE Trans. Power Electron.*, vol. 30, no. 5, pp. 2556–2569, May 2015.
[38] P. Dini, S. Saponara, S. Chakraborty, F. Hosseinabadi, and O. Hegazy, "Experimental characterization and electro-thermal modeling of double side cooled SiC MOSFETs for accurate and rapid power converter simulations," *IEEE Access*, vol. 11, pp. 79120–79143, 2023.
[39] S. M. I. Rahman, A. Moghassemi, A. Arsalan, L. Timilsina, P. K. Chamarthi, B. Papari, G. Ozkan, and C. S. Edrington, "Emerging trends and challenges in thermal management of power electronic converters: A state of the art review," *IEEE Access*, vol. 12, pp. 50633–50672, 2024.
[40] W. Hurley and W. Wolfle, *Transformers and Inductors for Power Electronics: Theory, Design and Applications*. Hoboken, NJ, USA: Wiley, 2013.
[41] E. Gurpinar and A. Castellazzi, "Single-phase T-type inverter performance benchmark using Si IGBTs, SiC MOSFETs, and GaN HEMTs," *IEEE Trans. Power Electron.*, vol. 31, no. 10, pp. 7148–7160, Oct. 2016.
[42] (2023). *Filter Product Information*. Accessed: Jan. 3, 2023. [Online]. Available: https://www.mtecorp.com/

HUSSAIN A. HUSSAIN (Member, IEEE) received the B.Sc. degree in electrical engineering from Kuwait University, Kuwait, in 2007, and the M.Sc. and Ph.D. degrees in electrical engineering from Texas A&M University, College Station, TX, USA, in 2012 and 2017, respectively.

He was with Kuwait National Petroleum Company (KNPC), Shuiaba Refinery, Kuwait, as a Design Engineer; and Texas Instruments, Dallas, TX, as a Research Engineer with the Kilby Laboratories. Currently, he is an Assistant Professor with the Electrical Engineering Department, Kuwait University. His research interests include designing and controlling multi-phase and linear machines, including sensorless control and fault control of electric machines. He is also interested in wide band gap (WBG) devices and distributed energy resources, including photovoltaic, wind, and hydropower.

JELENA LONCARSKI (Member, IEEE) received the B.Sc. and M.Sc. degrees in electrical engineering from the Faculty of Electrical Engineering, University of Belgrade, Serbia, in 2007 and 2010, respectively, and the Ph.D. degree in electrical engineering from the Department of Electrical Engineering, University of Bologna, Italy, in 2014.

She was a Researcher with the Department of Engineering Sciences, Division of Electricity, Uppsala University, Sweden; and the Department of Electrical and Information Engineering, Polytechnic University of Bari, Italy. She is currently an Assistant Professor of power electronics and drives with the Department of Electrical, Electronic, and Information Engineering "Guglielmo Marconi," University of Bologna. Her research interests include power electronic circuits and converters for electric drives and renewable energy sources, wide band gap (WBG) devices, electric vehicle charging systems, and sustainability.

LEPOSAVA B. RISTIC (Member, IEEE) received the B.Sc., M.Sc., and Ph.D. degrees from the University of Belgrade, Serbia, in 1990, 1999, and 2012, respectively.

She is an Associate Professor with the Department for Power Electronics and Drives, School of Electrical Engineering, University of Belgrade, where she teaches courses at all study levels. She has authored or co-authored over 100 papers, contributed to two book chapters, and co-authored three handbooks and two textbooks. Additionally, she has participated in several projects, coordinated a project for the National Ministry, and participated in an EU HORIZON project, along with various industry collaborations. Her primary research interests include the control of electrical drives, multi-motor drives, power electronics, and energy efficiency.

Dr. Ristic is a member of the Administrative Board of the Society for Power Electronics, Serbia and the Working Group at the Institute for Standardization of Serbia. She serves on the program and organizing committees of several international conferences. She was the Technical Chair at the IEEE PES PowerTech 2023 Conference, Belgrade. She is a reviewer of numerous international journals and a member of the editorial board of the journal *Electrical Engineering* (Springer).

ALBERTO BELLINI (Senior Member, IEEE) received the Laurea (M.S.) degree in electronic engineering and the Ph.D. degree in computer science and electronics engineering from the University of Bologna, Bologna, Italy, in 1994 and 1998, respectively.

From 1999 to 2004, he was with the University of Parma, Parma, Italy. He was an Honorary Scholar with the University of Wisconsin–Madison, Madison, WI, USA, in 2000. From 2004 to 2013, he was with the University of Modena and Reggio Emilia, Reggio Emilia, Italy. Since 2013, he has been a Professor of electric machines and drives with the Department of Electrical Engineering, University of Bologna. He is the author or co-author of more than 100 papers and one textbook and the holder of three industrial patents. His research interests include electric drive design and diagnosis, power electronics, and signal processing for industrial applications and sustainability. He was a recipient of the First Prize Paper Award from the Electric Machines Committee of the IEEE Industry Applications Society, in 2001.